UNIVERSITI MALAYSIA PERLIS
International Journal of Nanoelectronics and Materials
IJNeaM
ISSN 1985-5761 | E-ISSN 2232-1535

Characterization of carbon black and graphite filled epoxy conductive ink via green solvent method

Diana Mohamad Kamsani [a], *Zuliahani Ahmad* [a] *, *Helyati Abu Hassan Shaari* [a], *Pham Trung Kien* [b,c,d,e], and *Muhammad Mahyiddin Ramli* [f]

[a] *Faculty of Applied Sciences, Universiti Teknologi MARA (UiTM) Perlis Branch, 02600 Arau, Perlis, Malaysia*
[b] *Faculty of Materials Technology, Ho Chi Minh City University of Technology (HCMUT), Vietnam National University (VNUHCM), 268 Ly Thuong Kiet, District 10, Ho Chi Minh City, Vietnam*
[c] *Vietnam National University Ho Chi Minh City, Linh Trung Ward, Thu Duc District, Ho Chi Minh City, Vietnam*
[d] *Polymer Research Center, Ho Chi Minh City University of Technology (HCMUT), 268 Ly Thuong Kiet Street, District 10, Ho Chi Minh City, Vietnam*
[e] *VNU-HCM Key Laboratory for Material Technologies, Ho Chi Minh city University of Technology (HCMUT), 268 Ly Thuong Kiet Street, District 10, Ho Chi Minh City, Vietnam*
[f] *Institute of Nano Electronic Engineering (INEE), Universiti Malaysia Perlis (UniMAP), 01000 Kangar, Perlis, Malaysia*
∗ Corresponding author. Tel.: +6019-4153728; e-mail: zuliahani@uitm.edu.my

Received 09 March 2024, Revised 11 November 2024, Accepted 25 November 2024

ABSTRACT

Conductive ink is gaining attention in the electronics industry due to its affordability, simplicity, and environmentally friendly properties. This study aimed to analyze a conductive ink made with Carbon Black (CB) and Graphite (G) as fillers, with epoxy resin as the binder and a green co-solvent of ethanol and distilled water. Various characterization techniques were used to examine the fillers. X-ray diffraction (XRD) revealed that CB exhibited an amorphous region at the (002) peak around 21.1°, while G showed distinct peaks at 26.5° and 54.4°, indicating a well-ordered graphitic structure. UV-Vis analysis showed that both CB and G interacted with the epoxy matrix, with an absorption peak in the 270-280 nm range corresponding to π–π^* transitions. Fourier-transform infrared (FTIR) spectroscopy confirmed this interaction, with the presence of hydroxyl groups (2800–3500 cm^{-1}) and carboxyl group vibrations at 1241 cm^{-1}, indicating bonding between the polymer and filler. The dispersion of the fillers in the epoxy matrix was examined using Field Emission Scanning Electron Microscope (FESEM), which also assessed agglomeration. The ink's conductivity was tested according to ASTM F390 standards, with optimal CB loading at 4% achieving a conductivity of 4.49×10^{-5} S/m and optimal G loading at 3% yielding a conductivity of 7.14×10^{-5} S/m. These results indicate that G-based conductive ink with 3% loading performs better than CB-based ink for printed electronics applications.

Keywords: *Conductive ink, Epoxy, Carbon black, Graphite*

1. INTRODUCTION

The production of printed electronic devices, including displays, sensors, current collector grids, and RFID tags, has garnered significant attention. One major challenge in printed electronics is finding materials and processes that are both practical and eco-friendly, as many face obstacles preventing their use in commercial applications. A promising approach involves the use of conductive ink, a novel and cost-effective method for designing flexible electronics that seamlessly integrates with current manufacturing processes. The primary role of conductive ink is to serve as an interconnect, forming conductive regions [1]. Ideally, a high-quality conductive ink should exhibit excellent printability, low viscosity, stability, substrate adhesion, and high electrical conductivity both during and after printing processes. Typically composed of solvents, conductive fillers, and binder agents [2].

Epoxy resins, characterized by low manufacturing pressure, minimal cure shrinkage, and low residual stresses, are chosen for their unique manufacturing features [3]. With the appropriate curing agent, epoxy resins can be utilized over a broad temperature range to control cross-linking levels. Their appeal is further enhanced by excellent mechanical and adhesive properties, chemical resistance, and the versatility of available filler and curing agent options [4]. Epoxy, in its standalone form, lacks conductivity. Therefore, regulating the addition of conductive filler volume to the non-conductive matrix allows for a diverse range of electrical conductivities [5].

Carbon black (CB) is a general term for a family of small-sized, mostly amorphous, or paracrystalline carbon particles that aggregate to form various sizes and shapes [6]. Traditionally favored as a filler in elastomers, plastics, paints, and printing ink, carbon black is chosen for its ease of preparation, resulting in cost-effectiveness and favorable mechanical, electrical, and optical properties [7]. The reinforcement effect is influenced by interactions between polymer molecules, carbon black particles, and the polymer matrix, with the degree of carbon black dispersion and loading playing significant roles [6]. Although the conductivity of carbon black is not better than that of copper and silver, it can provide an effective alternative to electrical conductivity.

Graphite (G), a crystalline form of the element carbon, is composed of layered graphene sheets. These layers exhibit strong atomic bonding but are connected by relatively weak bonds. Graphite is found in nature or can be synthesized, and it is commonly employed as an electronically conducting filler due to its cost-effectiveness and natural abundance [8,9]. Its low density and cost make graphite and carbon preferable over metallic substances for similar purposes. Additionally, they possess the advantage of being generally inert and compatible with most polymer systems. The electrical conduction in carbon materials occurs through the pi bonding system among neighboring carbon atoms in the carbon/graphite structure, provide the pathway for energy transfer. The critical aspect of producing a conductive polymer lies in establishing a continuous pathway of interconnected conductive particles within the polymer.

Nanofillers have demonstrated remarkable performance compared to traditional fillers in enhancing conductivity at low concentrations. However, their tendency to clump together at higher concentrations, a result of strong self-interactions, hampers their practical use [9]. Both carbon black (CB) and graphite tend to clump together in water-based solvents and liquids that lack the necessary cohesive energies, due to their natural hydrophobic properties. [10]. To address this, the production of CB and G conductive ink involves using ethanol and distilled water as dispersing agents. Ethanol and water exhibit different polarities, enabling them to dissolve a wide array of compounds. Ethanol is a polar solvent, while water possesses high polarity due to its hydrogen bonding capabilities. This combination enhances the solubility of substances that might not dissolve well in either solvent alone [11]. The utilization of water and ethanol as eco-friendly solvents helps in reducing waste generation, offering a versatile, safe, and cost-effective option for various applications.

The objective of this study is to characterize conductive ink composed of epoxy filled with G and CB. Various formulations of Epoxy-CB and Epoxy-G were synthesized via the green co-solvent method with different loadings ranging from 0% to 5%. Furthermore, the study seeks to fill the gap in existing research by exploring the interactions that arise when fillers are integrated into the resin matrix, motivating the initiation of this research project.

2. MATERIAL AND METHODS

2.1. Materials and Instrumentation

The research utilized Bisphenol-A-(epichlorohydrin) epoxy resin, 3-aminomethyl-3,5,5-trimethylcyclohexylamine as the hardener, graphite with a particle size less than 20 µm acquired from Sigma Aldrich, carbon black N330 with a particle size of approximately 28-36 nm and a molar mass of 12.011 g/mol, Sodium Dodecyl Sulfate (SDS) as a surfactant with a particle size of around 110 µm obtained from R&M Malaysia, along with ethanol and distilled water. The instruments utilized included an X-Ray Diffractometer (XRD), UV-Vis Spectrophotometer, Perkin Elmer Spectrum RX1 Fourier-transform infrared (FTIR), Supra 55VP Field-emission scanning electron (FESEM), and a digital multimeter.

2.2. Preparation of Epoxy-CB and Epoxy-G Conductive Ink

G and CB were produced with distinct formulations tailored to different ink categories, as detailed in Table 1 and Table 2. The specified amounts of G and CB were incorporated into their respective mixtures of Bisphenol-A-(epichlorohydrin) epoxy resin, combined with a solvent mixture of ethanol and distilled water in a 2:1 ratio. Following the addition of SDS as a surfactant, the conductive ink mixture underwent mechanical stirring at 400 rpm for 5 minutes before introducing 3-aminomethyl-3,5,5-trimethylcyclohexylamine at a 2:1 epoxy/curing agent ratio. The components were then mixed using an ultrasonicator at room temperature for approximately 1 hour. For each ink formulation, some were directly analyzed with liquids, while the remainder were employed for film analysis. The produced epoxy-CB and epoxy-G inks are shown in Figure 1 and Figure 2, respectively.

2.3. Characterization Studies

To analyze the crystallographic structure of the conductive film, XRD analysis was performed utilizing a carbon X-ray source with a wavelength of 1.5–1.6 Å. The size of the crystallites was calculated by measuring the full width at half maximum (FWHM). The identification of functional groups in the prepared conductive ink samples was carried out using Perkin Elmer FTIR spectroscopy. The analysis was conducted with a resolution of 4 cm^{-1} within the range of 400 to 4000 cm^{-1}. As the sample was being prepared, it was evaluated for film formation. The FTIR analysis was employed to verify the presence of dispersed CB and

Table 1. Ink formulation of Epoxy-CB conductive ink

Formulation	Filler (g)	Epoxy (g)	Hardener (g)
Epoxy 0%	0.0	2	1
Epoxy-CB 1%	0.1	2	1
Epoxy-CB 2%	0.2	2	1
Epoxy-CB 3%	0.3	2	1
Epoxy-CB 4%	0.4	2	1
Epoxy-CB 5%	0.5	2	1

Table 2. Ink formulation of Epoxy-G conductive ink

Formulation	Filler (g)	Epoxy (g)	Hardener (g)
Epoxy 0%	0.0	2	1
Epoxy-G 1%	0.1	2	1
Epoxy-G 2%	0.2	2	1
Epoxy-G 3%	0.3	2	1
Epoxy-G 4%	0.4	2	1
Epoxy-G 5%	0.5	2	1

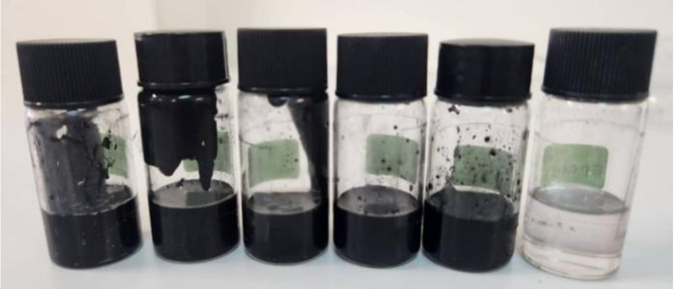

Figure 1. Epoxy-CB conductive ink produced with 0-5% (from right to left)

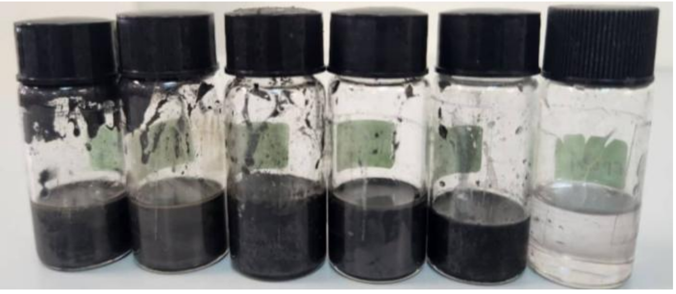

Figure 2. Epoxy-G conductive ink produced with 0-5% (from right to left)

G conductive fillers in the epoxy resin conductive ink. To assess the performance of dispersed conductive fillers, a UV-visible spectrometer was utilized. The absorbance mode was selected for measurement, and the evaluation was carried out within the wavelength range of 200-800 nm. This spectrometer proved to be an effective tool in this regard. FESEM was used to study the morphological structure of the conductive ink, with a particular focus on its dispersion characteristics and any potential agglomeration. The cross-section of the thin conductive film was prepared by cutting with nitrogen gas and coating it with a gold sputter layer for enhanced imaging clarity.

2.4. Conductivity Test

A digital multimeter was used to measure the conductivity of the conductive film, following the standard method outlined in ASTM F390, which is typically applied to thin films. The multimeter provided a real-time resistance reading, which was then converted into conductivity using Equation (1):

$$\sigma = A/(t \times R) \quad (1)$$

where R is the resistance measured by the multimeter (Ω), A is the cross-sectional area of the conductive film (m^2), t is the thickness of the conductive film (m), and σ is the conductivity (S/m).

3. RESULTS AND DISCUSSION

3.1. XRD Analysis

X-ray diffraction (XRD) is the standard method for investigating the microscopic structure of crystalline carbon materials [12]. The XRD profile in Figure 3 illustrates the distinctive patterns of CB and G. CB is typically amorphous and does not have a well-defined crystalline structure. It is composed of small, colloidal-sized particles primarily consisting of carbon atoms arranged in a disordered or amorphous manner. In contrast to G, amorphous carbon does not exhibit well-defined XRD peaks; rather, it displays a broad and featureless XRD pattern, indicative of the absence of a regular crystal lattice. The XRD pattern of CB reveals a notable high baseline and broad peak width. While the (002) peak of crystalline graphite is typically found at a 2θ angle of 26.5°, the corresponding peak of CB is observed at approximately 21.1°. This discrepancy suggests that the micro-crystallites in CB differ from those present in G [13]. In line with a study conducted by Nascimento et al., a lower intensity is observed at the peak of 22.5°, indicating the possible presence of amorphous regions [14]. The absence of sharp peaks further signifies that there is very little crystalline domain present in CB fillers, emphasizing their predominantly amorphous nature [15].

G, on the other hand, exhibits a well-organized crystalline structure. In XRD analysis, sharp diffraction peaks can be observed corresponding to the crystal planes of graphite. The most intense peak for G typically occurs at a 2θ value of approximately 26.5˚, corresponding to the (002) crystal plane [13]. The XRD pattern of G, depicted in Figure 3, exhibits two prominent peaks at 26.5° and 54.4°, which can be attributed to the (002) and (004) crystal planes, respectively [16]. This particular peak, notably tight and sharp at 2θ = 26.5°, which signifies the presence of a well-ordered graphitic structure. The intercellular spacing within the crystal lattice associated with this peak is measured to be 3.37 Å. The XRD data shows the typical crystal structure of G [17]. The characteristic (002) peak corresponding to the interlayer spacing between the graphene layers within the crystal lattice of graphite, affirming its highly ordered and layered composition. It is noteworthy that the broader subpeak at 21.1˚ is attributed to amorphous carbon, while the narrower subpeak at 26.5˚ points to a structured and well-ordered configuration [18]. The observed peak broadening in the G XRD pattern suggested that the stacking of G was not well ordered [19].

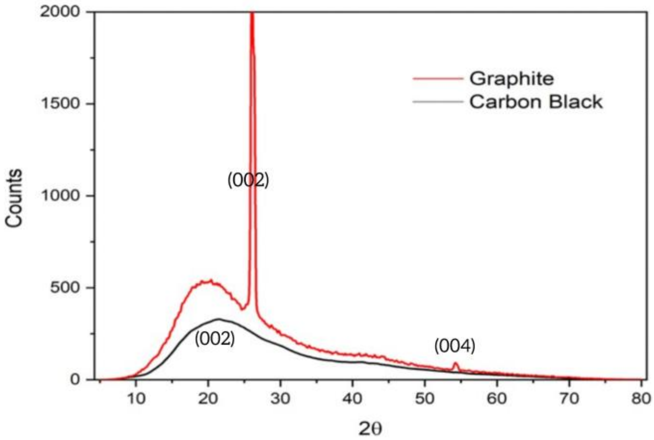

Figure 3. XRD pattern of CB and G

3.2. UV-Visible Spectrophotometer

This study utilized UV–Vis spectroscopy to investigate how conductive filler particles disperse within an epoxy matrix. The absorption peaks observed in a UV-Vis spectrum can yield insights into the bonding characteristics of a molecule. Specifically, the position and intensity of these absorption peaks can be linked to various electronic transitions, such as π to π* transitions (involving bonding pi to antibonding pi) or n to π* transitions (involving non-bonding to antibonding pi). The effectiveness of UV–visible spectroscopy in studying carbon materials is well-established, given the distinctive absorption patterns of these materials in the UV spectral range [20]. The UV-Visible spectra for epoxy and CB loadings are depicted in Figure 4(a). Within the UV-Vis range, epoxy displays lower absorbance and demonstrates the most significant shift in absorption wavelength within the 350-400 nm range. The process of epoxy polymeric substances absorbing light energy in the UV and visible spectra occurs when electrons transition from the n orbital to the π* orbital, moving from the ground state to higher energy states [21]. The low absorbance observed in the UV-Vis spectrum of epoxy is often attributed to the material's inherent transparency in both the visible and UV regions. This characteristic is consistent with findings from a study conducted by Mailhot et al., where the epoxy structure was noted to absorb light in the UV domain, with a peak around 340 nm [22].

The absorption characteristics are influenced by both the wavelength and the filler type. The UV absorption peak observed in carbon materials is caused by shifts in electrons between bonding and antibonding orbitals. When carbon materials absorb UV light, it's due to these electron shifts between bonding and antibonding π orbitals. The σ-σ* transitions usually happen in the far UV spectrum, approximately 60-100 nm, whereas the π–π* transitions occur in the range of 180-260 nm [20]. The π–π* transitions that result is expected to be caused by the larger surface area of the carbon compounds when exposed to UV light. Consequently, an increased absorption in the UV-visible spectra is anticipated by increasing the surface area of the dispersion [20]. This is evident in Figure 4(a), where the rise in UV–vis absorption from 0- 5% of CB can be explained by the total surface area of the CB aggregates following dispersion. Adding filler to the polymer enhances the peak intensity, as seen in the UV-Vis spectra of epoxy–CB. The UV-vis spectrum reveals that the most significant shift in absorption wavelength occurs in the 250-260 nm range, suggesting that polymeric materials undergo carbonization when exposed to radiation. The transition of the absorption edge from UV to the visible spectrum is likely due to an expansion in the length of conjugated structures [21].

The UV–Vis spectroscopy analysis of the G sample is depicted in Figure 4(b). The dispersion of G at various loadings exhibited a typical absorbance peak around 264 nm, characteristic of the π-plasmon absorption of G in the UV region. The peak observed at 264 nm is a result of the combined π-π* electronic transition of the closely packed aromatic rings within the graphene sheet [23]. The absorbance of G increased with higher loading content, indicating greater absorption of UV light by well-dispersed graphite flakes and sheets. This phenomenon suggested the existence of smaller and thinner graphite sheets and flakes, which had separated from the bulk graphite during the mechanical mixing process [24]. This observation aligns with the findings of Senthil et al. [25]. The dispersed G within the epoxy demonstrated the ability to interact with incident light, enhancing absorption through electronic transitions within the graphite structure. The absorbance may originate from conjugated aromatic systems within the graphite structure or any functional groups attached to graphite. Aromatic systems, such as benzene rings or polycyclic aromatic hydrocarbons (PAHs), can contribute to increased absorption in the UV region [26].

3.3. Fourier Transform-Infrared Spectroscopy (FTIR)

FTIR analysis was employed to identify functional groups in the sample and confirm the interaction between epoxy and conductive fillers. Figure 5 displays a comparative FTIR

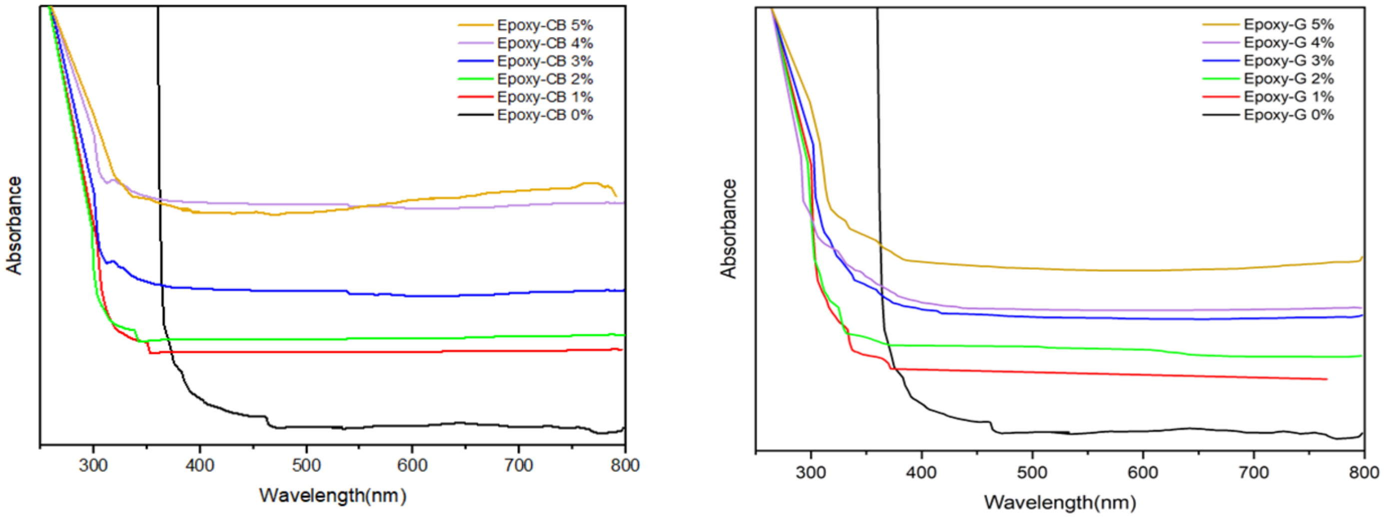

(a) (b)

Figure 4. UV-Vis spectra of (a) CB loadings and (b) G loadings

spectra of pure epoxy, pure CB, and pure G. The spectrum of pure epoxy resin displays typical absorption bands that are commonly found in a bisphenol-A-(epichlorohydrin) epoxy resin. There is a noticeable absorption band representing the OH bond, visible between 3500 and 2800 cm^{-1}, with a weak peak at 3664 cm^{-1} indicating stretching vibrations of "free" O-H groups. However, this peak is relatively small due to the limited number of OH groups present in the resin molecule. [27]. The 1250-1000 cm^{-1} range exhibits aliphatic C-O stretching and the aromatic ether group C-O-C of the epoxy ring. In the 1600-1400 cm^{-1} range, a peak corresponds to C=C stretching vibrations. The absorption at 2970 cm^{-1} is due to C-H vibrations, while the 826 cm^{-1} band corresponds to the distinctive out-of-plane bending vibration of C-H within the benzene ring. Importantly, the absence of residual absorption at 3380 cm^{-1} (NH_2) in the pure epoxy spectrum suggests that all the amine groups have undergone reaction during the curing process [22].

While, in pure CB, the hydroxyl groups present in the material produce -OH stretching vibrations, represented by the band at 3085 cm^{-1}. The peaks at 2736 cm^{-1}, 1785 cm^{-1}, and 1630 cm^{-1} correspond to -CH vibrations, C=O stretching, and C=C stretching, respectively, indicating the activation of CB in the area [28]. The peak observed at 1208 cm-1 in the IR spectrum is attributed to the stretching of C-O bonds. Through FTIR analysis, this study suggests that CB contains both hydroxyl (–OH) and carboxyl (–COO–) functional groups [29]. In FTIR spectra G, a vibration related to -CH occurs at 2974 cm^{-1}. Additionally, other peaks are noticeable, such as C=C stretching vibrations at 1623 cm^{-1}, C-C at 1457 cm^{-1}, and C–O stretching vibrations at 1259 cm^{-1}.These peaks are not prominent due to their low transmittance compared to epoxy.

The FTIR results depicted in Figures 6(a) and (b) elucidate the characteristics of pure epoxy as well as epoxy reinforced with varying concentrations of CB and G. Notably, there is no emergence of new peaks following the reinforcement by both CB and G fillers. Furthermore, there is an absence of peak shifts, and the intensity of all composite peak characteristics increased as the concentration of filler content increased. In the bonding mechanism, amine-cured epoxy resins predominantly form bonds with the surface of carbon fillers through hydrogen interactions. These interactions take place between the amino or epoxy groups of the polymer and the hydroxyl or carboxyl groups of the filler. The interface between the filler and resin suggests possible molecular arrangements for these hydrogen and covalent bonds, as suggested by Horie et al. in 1976 [30]. The presence of hydroxyl groups, observed in the band between 2800 cm^{-1} and 3500 cm^{-1}, and the formation vibration of the carboxyl group at 1241 cm^{-1} support the establishment of these bonds. With the addition of fillers, the intensity of the carboxyl group increases, indicating the formation of covalent bonds. Analyzing particular peaks, the region from 1600 to 1400 cm^{-1} is linked with the stretching vibrations of C=C in vinyl ether and C–C stretching in an aromatic ring. Meanwhile, the spectral range from 1250 to 1000 cm^{-1} is associated with the C-O-C stretching vibrations of an epoxy group. This spectral analysis affirms the successful incorporation and bonding of both CB and G fillers with the polymer matrix. However, in the case of CB filler, as shown in Figure 6(a), the signal for 5% loading content is diminished. This reduction is likely attributed to the size of CB, which might have led to a reduction in both the pore volume and surface area of the polymer matrix, as suggested by Zappielo et al. in 2016 [31].

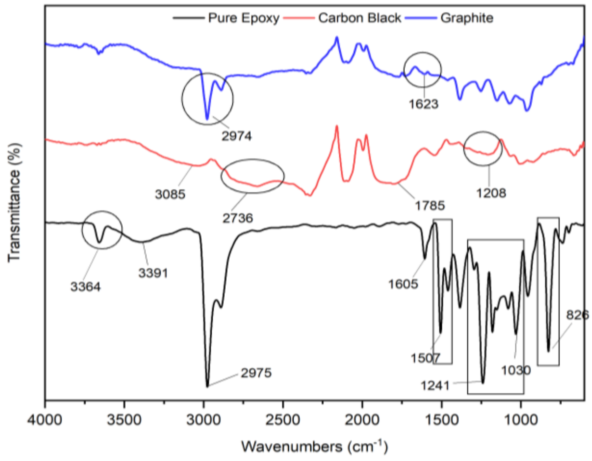

Figure 5. FTIR spectrum for pure epoxy, pure CB and pure G

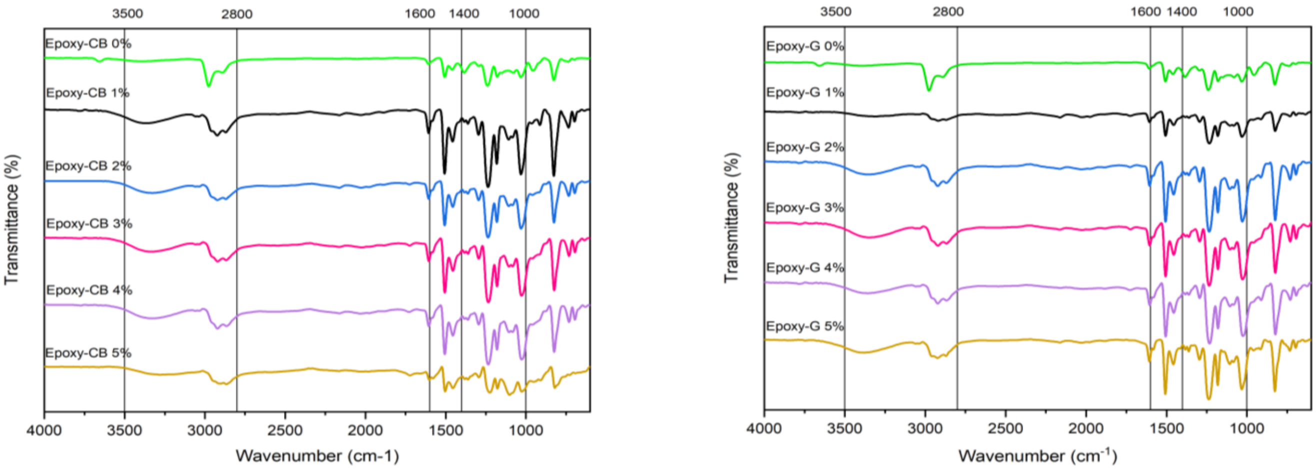

(a) (b)

Figure 6. FTIR spectrum of various loadings of (a) CB and (b) G

3.4. Field Emission Scanning Electron Microscope (FESEM)

Figure 7 shows FESEM cross-sectional images of fractured neat epoxy, Epoxy-CB, and Epoxy-G conductive films, all taken at the same magnification to examine the internal distribution of conductive particles within the epoxy matrix. In the neat epoxy sample, which contains no fillers, the fracture surface appears smooth, as shown in Figure 7(a), highlighting the brittle nature typical of epoxy resin. This smoothness is a characteristic feature of neat epoxy morphology, indicating low fracture toughness [32]. Conversely, when the epoxy is reinforced with fillers, the fracture surfaces tend to appear rougher or more textured, reflecting an increase in fracture toughness. This textured morphology suggests that the fillers enhance energy dissipation and crack resistance, thereby improving the material’s durability and structural performance.

The FESEM images of Epoxy-CB shown in Figures 7(b) and (c) display typical spherical CB particles that form larger chain-like or fractal aggregates. This observation indicates a natural tendency for clustering due to intermolecular forces, such as hydrogen bonding. The influence of surface functional groups, including hydroxyl, carbonyl, and carboxyl, is supported by FTIR data [33]. At lower concentrations of CB (Figure 7b), the dispersion appears more irregular, with clusters forming inconsistently throughout the matrix. In contrast, the Epoxy-CB sample at 4% concentration (Figure 7c) exhibits a relatively uniform distribution, with particles organized into a continuous conductive network [34]. This homogeneous dispersion likely enhances conductivity by maximizing the contact area between the CB particles and the epoxy, thereby promoting bridging networks that facilitate electron transfer. These findings suggest that a 4% CB concentration is optimal, providing adequate distribution without leading to excessive aggregation, which could otherwise hinder the material's conductive properties [35].

The morphology of G exhibits a distinctive flake-like structure with uneven formation [34]. As shown in Figure 7(d), at a G content of 1%, the dispersion of G within an epoxy polymer matrix is poor, leading to the stacking of graphene platelets due to their insolubility in the matrix and the strong Van der Waals forces between layers. In contrast, when the G content is increased to the optimal level of 3%, the graphene flakes do not adhere to one another; instead, they are embedded within and adhere to the matrix, as illustrated in Figure 7(e) [36]. This enhanced distribution is likely a result of the mechanical mixing process, which uses shear stresses to reduce the lateral dimensions of the 2D filler and exfoliate the graphene, resulting in thinner structure [37]. Figure 7(e) indicates that a higher G content improves the contact between conductive fillers, thereby enhancing conductivity. However, slight agglomeration begins to occur when the filler content exceeds 3%, which could negatively impact dispersion and stability in conductive inks.

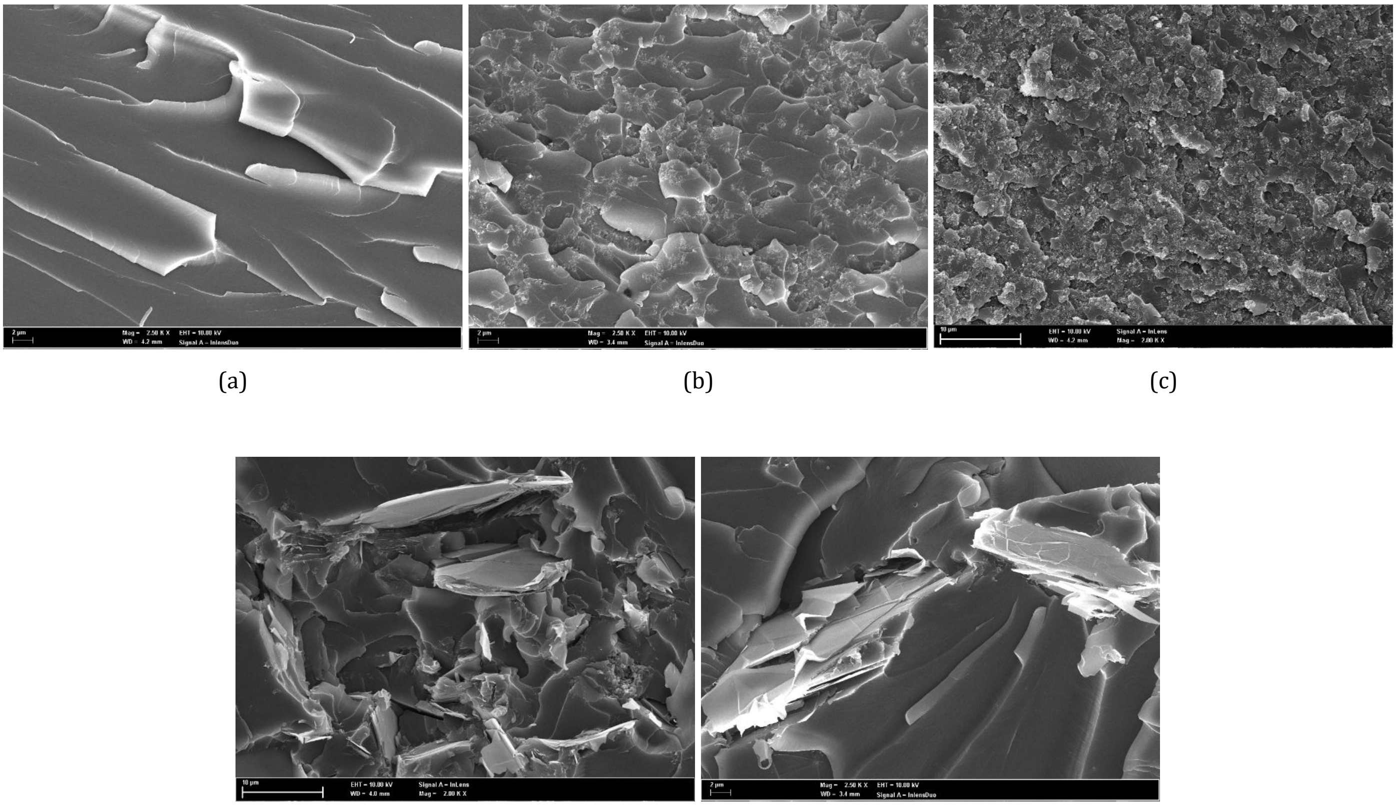

(a) (b) (c)

(d) (e)

Figure 7. FESEM micrographs of conductive ink (a) Neat Epoxy (b) Epoxy-CB 1% (c) Epoxy-CB 4% (d) Epoxy-G 1% (e) Epoxy-G 3% at 2500X magnification

3.5. Conductivity Performance

The electrical characteristics of the samples were evaluated using a two-point probe method with a digital multimeter. Bulk resistivity values were manually recorded from live multimeter readings. These resistance measurements were then converted to resistivity, and conductivity was subsequently calculated using Equation 1. Tables 3 and 4 present the multimeter resistance readings along with the average thickness of all film samples. As conductivity and resistivity is inversely related, a decrease in resistivity corresponds to an increase in conductivity, and vice versa.

The graphs depicted in Figure 8 and Figure 9 show the correlation between the resistivity and conductivity of CB loading and G loading respectively. The resistance of the control sample without any filler is significantly low, displaying "OL," which likely indicates that the measured value exceeds the maximum range that the multimeter can display. As the concentration of Epoxy-CB increases from 0% to 4%, conductivity gradually rises from 0 S/m to 4.49×10^{-5} S/m. The trend illustrates in Figure 8 demonstrate how CB loading enhances the conductivity of the epoxy matrix. At low concentrations, CB particles are too dispersed to form continuous conductive paths, resulting in low conductivity. The epoxy matrix maintains a stable dispersion of particles, with no clustering observed, as shown in Figure 7(a). As the concentration increases, the particles come closer together, forming continuous networks or clusters. At 4% CB loading, the optimum loading is reached, resulting in a sudden decrease in resistivity and yielding the best electrical performance at 4.49×10^{-5} S/m. Beyond this optimal point, there is a slight decrease in conductivity due to the transition from dispersed to agglomerated CB particles, as shown in Figure 7(c) [38]. Agglomerates form as CB particles cluster due to van der Waals forces, indicating poor dispersion between the epoxy and CB fillers [39]. At 5% CB loading, resistivity peaks, resulting in the highest resistivity and lowest conductivity among all CB-reinforced samples, likely due to the agglomeration phenomenon.

Table 3. Resistance reading, thickness and conductivity of Epoxy-CB loadings

Formulation	Resistance (MΩ)	Thickness (m)	Conductivity (S/m)
Epoxy 0%	OL	$8.1 \times 10^{-4} \pm 0.5$	0
Epoxy-CB 1%	2.792	$7.0 \times 10^{-4} \pm 0.5$	2.05×10^{-5}
Epoxy-CB 2%	2.361	$7.2 \times 10^{-4} \pm 0.5$	2.35×10^{-5}
Epoxy-CB 3%	2.224	$7.2 \times 10^{-4} \pm 0.5$	2.50×10^{-5}
Epoxy-CB 4%	1.273	$7.0 \times 10^{-4} \pm 0.5$	4.49×10^{-5}
Epoxy-CB 5%	1.701	$7.6 \times 10^{-4} \pm 0.5$	3.09×10^{-5}

Table 4. Resistance reading, thickness and conductivity of Epoxy-G loadings

Formulation	Resistance (MΩ)	Thickness (m)	Conductivity (S/m)
Epoxy 0%	OL	$8.1 \times 10^{-4} \pm 0.5$	0
Epoxy-G 1%	2.651	$6.8 \times 10^{-4} \pm 0.5$	2.22×10^{-5}
Epoxy-G 2%	1.857	$6.9 \times 10^{-4} \pm 0.5$	3.12×10^{-5}
Epoxy-G 3%	0.778	$7.2 \times 10^{-4} \pm 0.5$	7.14×10^{-5}
Epoxy-G 4%	0.962	$7.4 \times 10^{-4} \pm 0.5$	5.62×10^{-5}
Epoxy-G 5%	1.082	$7.5 \times 10^{-4} \pm 0.5$	4.93×10^{-5}

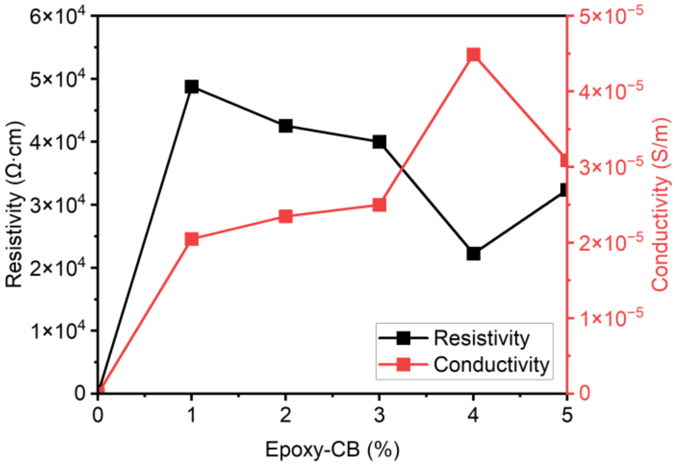

Figure 8. Resistivity vs conductivity using multimeter of Epoxy-CB

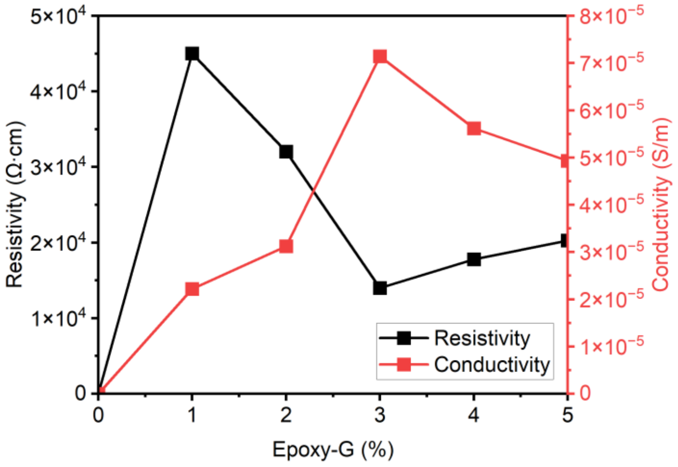

Figure 9. Resistivity vs conductivity using multimeter of Epoxy-G

The same trend is observed for G filler particles in Figure 9, where the optimal conductivity level is attained at a loading of 3%, resulting in a value of 7.14×10^{-5} S/m. At this ideal concentration, the dispersion of G within the epoxy matrix is adequate, as indicated by the thinner structures of the G platelets, which do not appear to be stacked together, as shown in Figure 7(e). According to Yan et al., the high surface area-to-volume ratio of graphite promotes increased contact points between graphene sheets and the epoxy matrix, enhancing electron transfer [40]. However, conductivity decreases at 4% and 5% loading of Epoxy-G, likely due to agglomeration phenomena within the epoxy matrix. Cilento et al., note that excessive G loading can disrupt the continuity of the epoxy matrix [41]. G particles can create holes, voids, or defects that impede electron flow, thereby reducing overall conductivity. As G loading increases, achieving an even dispersion of the particles becomes more difficult. Poor dispersion and uneven distribution lead to increased electron scattering, ultimately diminishing the effective conductivity of the composite. A homogeneous dispersion of G within the epoxy matrix is crucial for achieving excellent conductivity, as it enables the G particles to maintain close contact with one another.

4. CONCLUSION

In conclusion, this study provides a comprehensive analysis of the characterization of different carbon black and graphite loadings ranging from 0% to 5% in epoxy resin conductive ink. The presence of CB and G in epoxy resin was determined through XRD, FTIR, and UV-Vis analyses. From the XRD analysis, the (002) peak for CB is situated around 21.1°, indicating the possible presence of amorphous regions. This confirms the structure of CB, as CB is typically amorphous and does not have a well-defined crystalline structure. Graphite, on the other hand, exhibits a well-organized crystalline structure. The XRD pattern of graphite shows two strong peaks at 26.5° and 54.4°, which are attributed to the (002) and (004) crystal planes, indicating the existence of a highly organized graphitic arrangement. The UV-Vis analysis revealed an interaction between the epoxy matrix and both conductive fillers, CB and G, as evidenced by an absorption peak in the 270-280 nm range, attributed to π–π^* transitions. The UV absorption peak found in carbon materials arises from transitions between bonding and antibonding orbitals of electrons, commonly detected at approximately 280 nm. FTIR testing further confirmed the interaction between epoxy and carbon conductive fillers. The interactions are expected to occur between the amino or epoxy groups of the polymer and the conductive fillers through the hydroxyl or carboxyl groups. The presence of OH groups, observed in the band between 2800 cm^{-1} and 3500 cm^{-1}, and the vibrational formation of the carboxyl group at 1241 cm^{-1} support the establishment of these bonds. FESEM was utilized to analyze the internal distribution of conductive particles within the epoxy matrix. A uniform dispersion of conductive fillers within the matrix was found to enhance conductivity. It was determined that a CB loading of 4% provided optimal performance, achieving the highest conductivity of 4.49×10^{-5} S/m as measured by a multimeter. Similarly, a graphene G content of 3% was found to be optimal, yielding a peak conductivity of 7.14×10^{-5} S/m. Therefore, the G filler with a 3% loading was determined to be the best option compared to the CB, offering both enhanced conductivity and a more homogeneous distribution.

ACKNOWLEDGMENTS

This work was supported by GERAN INSENTIF PENYELIAAN (GIP) of Universiti Teknologi MARA, Malaysia (PY/2022/01146). The author would like to thank Faculty of Applied Sciences (FSG), Universiti Teknologi MARA (UiTM) Perlis for providing the facilities and laboratory materials used in this research project.

REFERENCES

[1] H. Saad, A. N. S. Fiza, M. A. Salim, M. R. Mansor, and A. N. A. Yahaya, “Electrical Characterization of Graphene Nanoparticles Conductive Ink using Thermoplastic Polyurethane (TPU) Substrate,” *5International Journal of Advanced Research in Engineering Innovation*, vol. 3, no. 2, pp. 58–68, 2021.

[2] H. Saad, M. A. Salim, N. A. Masripan, A. Md. Saad, and F. Dai, “Nanoscale Graphene Nanoparticles Conductive Ink Mechanical Performance Based on Nanoindentation Analysis,” *International Journal of Nanoelectronics and Materials (IJNEAM)*, vol. 13 (Special Issue), pp. 439–448, May 2020.

[3] H. Sukanto, W. W. Raharjo, D. Ariawan, J. Triyono, and M. Kaavesina, “Epoxy resins thermosetting for mechanical engineering,” *Open Engineering*, vol. 11, no. 1, pp. 797–814, Jul. 2021, doi: 10.1515/eng-2021-0078.

[4] Y. Guo, Y. Liu, J. Liu, J. Zhao, H. Zhang, and Z. Zhang, “Shape memory epoxy composites with high mechanical performance manufactured by multi-material direct ink writing,” *Composites Part A: Applied Science and Manufacturing*, vol. 135, p. 105903, Aug. 2020, doi: 10.1016/j.compositesa.2020.105903.

[5] B. Alemour, M. H. Yaacob, H. N. Lim, and M. R. Hassan, “Review of Electrical Properties of Graphene Conductive Composites,” *International Journal of Nanoelectronics and Materials (IJNEAM)*, vol. 11, no. 4, pp. 371–398, Oct. 2018.

[6] M. E. Spahr, R. Gilardi, and D. Bonacchi, “Carbon Black for Electrically Conductive Polymer Applications,” in *Fillers for Polymer Applications*, R. Rothon, Ed., Springer, 2017, pp. 375–400. doi: 10.1007/978-3-319-28117-9_32.

[7] H. Oxfall, G. Ariu, T. Gkourmpis, R. W. Rychwalski, and M. Rigdahl, “Effect of carbon black on electrical and rheological properties of graphite nanoplatelets/poly(ethylene-butyl acrylate) composites,” *Express Polymer Letters*, vol. 9, no. 1, pp. 66–76, 2015, doi: 10.3144/expresspolymlett.2015.7.

[8] M. D. S. Hajar, A. G. Supri, M. P. M. Hanif, and M. I. M. Yazid, “Effect of graphite loading on the electrical and mechanical properties of Poly (Ethylene Oxide)/Poly (Vinyl Chloride) polymer films,” *Journal of Physics: Conference Series*, vol. 908, p. 012020, Oct. 2017, doi: 10.1088/1742-6596/908/1/012020.

[9] H. Mohammad, A. A. Stepashkin, and V. v. Tcherdyntsev, “Effect of Graphite Filler Type on the Thermal Conductivity and Mechanical Behavior of Polysulfone-Based Composites,” *Polymers*, vol. 14, no. 3, p. 399, Jan. 2022, doi: 10.3390/polym14030399.

[10] A. P. S. Chauhan and K. Chawla, “Comparative studies on Graphite and Carbon Black powders, and their dispersions,” *Journal of Molecular Liquids*, vol. 221, pp. 292–297, Sep. 2016, doi: 10.1016/j.molliq.2016.05.043.

[11] L. Lajoie, A.-S. Fabiano-Tixier, and F. Chemat, “Water as Green Solvent: Methods of Solubilisation and Extraction of Natural Products—Past, Present and Future Solutions,” *Pharmaceuticals*, vol. 15, no. 12, p. 1507, Dec. 2022, doi: 10.3390/ph15121507.

[12] A. N. Popova, “Crystallographic analysis of graphite by X-Ray diffraction,” *Coke and Chemistry*, vol. 60, no. 9, pp. 361–365, Sep. 2017, doi: 10.3103/S1068364X17090058.

[13] S.-M. Lee, S.-H. Lee, and J.-S. Roh, “Analysis of Activation Process of Carbon Black Based on Structural Parameters Obtained by XRD Analysis,” *Crystals*, vol. 11, no. 2, p. 153, Feb. 2021, doi: 10.3390/cryst11020153.

[14] N. R. do Nascimento, I. F. Pinheiro, G. F. Alves, L. H. I. Mei, J. C. de Macedo Neto, and A. R. Morales, “Role of cellulose nanocrystals in epoxy-based nanocomposites: mechanical properties, morphology and thermal behavior,” *Polímeros*, vol. 31, no. 3, 2021, doi: 10.1590/0104-1428.20210057.

[15] S. C. Peterson, “Carbon Black Replacement in Natural Rubber Composites Using Dry-Milled Calcium Carbonate, Soy Protein, and Biochar,” *Processes*, vol. 10, no. 1, p. 123, Jan. 2022, doi: 10.3390/pr10010123.

[16] W. Dong *et al.*, “Acetylated SEBS Enhanced DC Insulation Performances of Polyethylene,” *Polymers*, vol. 11, no. 6, p. 1033, Jun. 2019, doi: 10.3390/polym11061033.

[17] R. Siburian, H. Sihotang, S. Lumban Raja, M. Supeno, and C. Simanjuntak, “New Route to Synthesize of Graphene Nano Sheets,” *Oriental Journal of Chemistry*, vol. 34, no. 1, pp. 182–187, Feb. 2018, doi: 10.13005/ojc/340120.

[18] J. Li, Y. Qin, Y. Chen, J. Shen, Y. Song, and Z. Wang, “Structural characteristics and evolution of meta-anthracite to coaly graphite: A quantitative investigation using X-ray diffraction, Raman spectroscopy, and high-resolution transmission electron microscopy,” *Fuel*, vol. 333, p. 126334, Feb. 2023, doi: 10.1016/j.fuel.2022.126334.

[19] F. T. Johra, J.-W. Lee, and W.-G. Jung, “Facile and safe graphene preparation on solution based platform,” *Journal of Industrial and Engineering Chemistry*, vol. 20, no. 5, pp. 2883–2887, Sep. 2014, doi: 10.1016/j.jiec.2013.11.022.

[20] M. Sharif Sh., F. Golestani Fard, E. Khatibi, and H. Sarpoolaky, “Dispersion and stability of carbon black nanoparticles, studied by ultraviolet–visible spectroscopy,” *Journal of the Taiwan Institute of Chemical Engineers*, vol. 40, no. 5, pp. 524–527, Sep. 2009, doi: 10.1016/j.jtice.2009.03.006.

[21] A. I. Al-Mosawi, M. H. Al-Maamori, and K. H. AL-Mayalee, “Spectroscopic Studies of Polyester – Carbon Black Composites,” *Research Journal of Material Sciences* , vol. 1, no. 2, pp. 10–14, Mar. 2013.

[22] B. Mailhot, S. Morlat-Thérias, M. Ouahioune, and J. Gardette, “Study of the Degradation of an Epoxy/Amine Resin, 1,” *Macromolecular Chemistry and Physics*, vol. 206, no. 5, pp. 575–584, Mar. 2005, doi: 10.1002/macp.200400395.

[23] F. Hof *et al.*, “Conductive inks of graphitic nanoparticles from a sustainable carbon feedstock,” *Carbon*, vol. 111, pp. 142–149, Jan. 2017, doi: 10.1016/j.carbon.2016.09.052.

[24] N. Komrapit, W. Punyodom, and P. Worajittiphon, “Compatibilizing and reinforcing an immiscible blend based on poly(lactic acid) with delaminated graphite: From raw graphite to enhanced polymer mechanical properties,” *Journal of Applied Polymer Science*, vol. 135, no. 42, Nov. 2018, doi: 10.1002/app.46821.

[25] R. A. Senthil, A. Selvi, P. Arunachalam, L. S. Amudha, J. Madhavan, and A. M. Al-Mayouf, “A sensitive electrochemical detection of hydroquinone using newly synthesized α-Fe_2O_3-graphene oxide nanocomposite as an electrode material,” *Journal of Materials Science: Materials in Electronics*, vol. 28, no. 14, pp. 10081–10091, Jul. 2017, doi: 10.1007/s10854-017-6769-x.

[26] B. Shi, D. Nachtigallová, A. J. A. Aquino, F. B. C. Machado, and H. Lischka, “High-level theoretical benchmark investigations of the UV-vis absorption spectra of paradigmatic polycyclic aromatic hydrocarbons as models for graphene quantum dots,” *The Journal of Chemical Physics*, vol. 150, no. 12, Mar. 2019, doi: 10.1063/1.5086760.

[27] I. J. Fernandes, R. V. Santos, E. C. A. dos Santos, T. L. A. C. Rocha, N. S. Domingues Junior, and C. A. M. Moraes, “Replacement of Commercial Silica by Rice Husk Ash in Epoxy Composites: A Comparative Analysis,” *Materials Research*, vol. 21, no. 3, Apr. 2018, doi: 10.1590/1980-5373-mr-2016-0562.

[28] R. I. Sugatri, Y. C. Wirasadewa, K. E. Saputro, E. Y. Muslih, R. Ikono, and M. Nasir, “Recycled carbon black from waste of tire industry: thermal study,” *Microsystem Technologies*, vol. 24, no. 1, pp. 749–755, Jan. 2018, doi: 10.1007/s00542-017-3397-6.

[29] C. Y. Liu and W. T. Cheng, “Surface modification and characterization of carbon black through oxidation,” *Surface and Interface Analysis*, vol. 51, no. 3, pp. 316–325, Mar. 2019, doi: 10.1002/sia.6581.

[30] K. Horie, M. Hiromichi, and I. Mita, “Bonding of epoxy resin to graphite fibres,” *Fibre Science and Technology*, vol. 9, no. 4, pp. 253–264, Oct. 1976, doi: 10.1016/0015-0568(76)90008-7.

[31] C. D. Zappielo *et al.*, “Solid Phase Extraction to On-Line Preconcentrate Trace Cadmium Using Chemically Modified Nano-Carbon Black with 3-Mercaptopropyltrimethoxysilane,” *Journal of the Brazilian Chemical Society*, 2016, doi: 10.5935/0103-5053.20160052.

[32] M. R. Zakaria, M. H. Abdul Kudus, H. Md. Akil, and M. H. Zamri, “Improvement of Fracture Toughness in

Epoxy Nanocomposites through Chemical Hybridization of Carbon Nanotubes and Alumina," *Materials*, vol. 10, no. 3, p. 301, Mar. 2017, doi: 10.3390/ma10030301.

[33] T. C. Cândido, A. C. Pereira, and D. N. da Silva, "Development and Characterization of Conductive Ink Composed of Graphite and Carbon Black for Application in Printed Electrodes," *Analytica*, vol. 4, no. 4, pp. 513–526, Dec. 2023, doi: 10.3390/analytica4040035.

[34] Q. Zhang, J. Wang, B.-Y. Zhang, B.-H. Guo, J. Yu, and Z.-X. Guo, "Improved electrical conductivity of polymer/carbon black composites by simultaneous dispersion and interaction-induced network assembly," *Composites Science and Technology*, vol. 179, pp. 106–114, Jul. 2019, doi: 10.1016/j.compscitech.2019.05.008.

[35] J. Zhang, M. Ahmadi, M. Serra, E. Jimenez-Pique, L. Llanes, and G. Fargas, "Integration of conductive silver sensors on zirconia ceramics by screen-printing for monitoring strain under applied load," *Ceramics International*, vol. 49, no. 7, pp. 11579–11588, Apr. 2023, doi: 10.1016/j.ceramint.2022.12.005.

[36] S. Daneshpayeh, F. A. Ghasemi, and I. Ghasemi, "The effect of nanoparticles shape on the mechanical properties of poly lactic acid matrix," *Journal of Elastomers & Plastics*, vol. 53, no. 6, pp. 684–697, Oct. 2021, doi: 10.1177/0095244320988168.

[37] F. R. Lamastra *et al.*, "Toward a better understanding of multifunctional cement-based materials: The impact of graphite nanoplatelets (GNPs)," *Ceramics International*, vol. 47, no. 14, pp. 20019–20031, Jul. 2021, doi: 10.1016/j.ceramint.2021.04.012.

[38] T. Prasse, L. Flandin, K. Schulte, and W. Bauhofer, "*In situ* observation of electric field induced agglomeration of carbon black in epoxy resin," *Applied Physics Letters*, vol. 72, no. 22, pp. 2903–2905, Jun. 1998, doi: 10.1063/1.121454.

[39] A. Kasgoz, D. Akın, and A. Durmus, "Rheological and electrical properties of carbon black and carbon fiber filled cyclic olefin copolymer composites," *Composites Part B: Engineering*, vol. 62, pp. 113–120, Jun. 2014, doi: 10.1016/j.compositesb.2014.02.017.

[40] Z. Yan, W. Yao, L. Hu, D. Liu, C. Wang, and C.-S. Lee, "Progress in the preparation and application of three-dimensional graphene-based porous nanocomposites," *Nanoscale*, vol. 7, no. 13, pp. 5563–5577, 2015, doi: 10.1039/C5NR00030K.

[41] F. Cilento, A. Martone, M. G. Pastore Carbone, C. Galiotis, and M. Giordano, "Nacre-like GNP/Epoxy composites: Reinforcement efficiency vis-à-vis graphene content," *Composites Science and Technology*, vol. 211, p. 108873, Jul. 2021, doi: 10.1016/j.compscitech.2021.108873.